View Online / Journal Homepage / Table of Contents for this issue
Dynamic Article Links

Nanoscale

Cite this: *Nanoscale*, 2012, **4**, 5965

www.rsc.org/nanoscale

PAPER

Halogen bonds in 2D supramolecular self-assembly of organic semiconductors†

Rico Gutzler,*[ab] Chaoying Fu,[ba] Afshin Dadvand,[ba] Yun Hua,[ab] Jennifer M. MacLeod,[a] Federico Rosei*[a] and Dmitrii F. Perepichka*[b]

Received 27th June 2012, Accepted 20th July 2012
DOI: 10.1039/c2nr31648j

Weak interactions between bromine, sulphur, and hydrogen are shown to stabilize 2D supramolecular monolayers at the liquid–solid interface. Three different thiophene-based semiconducting organic molecules assemble into close-packed ultrathin ordered layers. A combination of scanning tunneling microscopy (STM) and density functional theory (DFT) elucidates the interactions within the monolayer. Electrostatic interactions are identified as the driving force for intermolecular Br···Br and Br···H bonding. We find that the S···S interactions of the 2D supramolecular layers correlate with the hole mobilities of thin film transistors of the same materials.

Downloaded by Institut nationale de la recherche scientifique (INRS) on 17 September 2012
Published on 16 August 2012 on http://pubs.rsc.org | doi:10.1039/C2NR31648J

Introduction

Weak intermolecular interactions are the glue that holds together supramolecular crystalline structures made from organic molecules.[1–4] They form the basis of two-dimensional self-assembled surface-confined structures and as such are responsible for form and function of organic monolayers.[5–9] The literature on 2D molecular self-assembly at the liquid–solid interface is dominated by structures that are stabilized by van-der-Waals forces[10–13] and hydrogen bonds,[4,14–18] although other interaction schemes like π–π stacking[19–21] have also been reported. Halogen bonding (X-bonding), despite its importance in 3D crystal engineering,[22–24] has been studied less extensively in 2D self-assembly at the liquid–solid interface[25–29] or under ultra-high vacuum conditions.[30–34] Recent interest in X-bonding motivated its use as a binding motif in organic thin films[35] and as linker in the assembly of nanoparticles.[36] The importance of studying these interactions originates in the ability to tune the HOMO–LUMO gap of organic semiconductors: halogenation of these molecules lowers their electronic gap, but concomitantly perturbs their crystal structure in the solid state by introducing the possibility for halogen bonding.[37] Furthermore, X-bonds and hydrogen bonds (H-bonds) can act orthogonally to each other at the same bond acceptor,[38] which leads to particular three-centre binding motifs.[39,40] The X-bond is inherently more suitable for the assembly of semiconductors as it does not involve any acidic/basic centres that can trap charges (which would be the case in OH/NH containing building blocks). Studying their arrangement and how these molecules interact can thus be important for the understanding of organic electronic devices.[41]

Halogen bonds occur due to polarisation of the halogen atom in a C–X bond and the resulting non-spherical charge distribution and electrostatic potential. Charge depletion of the tip of the halogen atom produces a slight positive partial charge δ^+, while an equatorial ring around the C–X bond is partially negatively charged δ^- (Fig. 1a).[42,43] This characteristic positive electrostatic potential at the X-atom tip is called the σ-hole.[44] A halogen atom can thus interact with an electrophile and a nucleophile at the same time. This can lead to attractive interactions between two C–X fragments as depicted in Fig. 1b.[42,43] The X-bond is a result

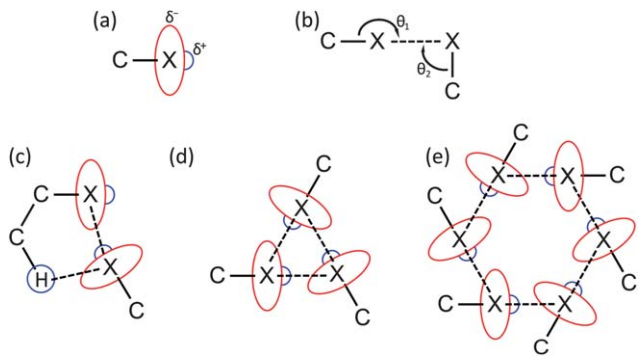

Fig. 1 X-bond interaction schemes. (a) Charge distribution in C–X bond with positive potential on the tip (blue) and a negative potential in the equatorial region (red) of the X-atom. (b) General X-bond interaction scheme with $\theta_1 \approx 150°–180°$ and $\theta_2 \approx 90°–120°$ according to ref. 42 and 43. (c) Combined X-bond and H-bond in three-centre binding motif (X_2H synthon). (d) Trimeric X_3 synthon. (e) Hexameric X_6 synthon.

[a]*Institut National de la Recherche Scientifique and Centre for Self-Assembled Chemical Structures, Université du Québec, 1650 boulevard Lionel-Boulet, Varennes, QC J3X 1S2, Canada. E-mail: gutzler@emt.inrs.ca; rosei@emt.inrs.ca*
[b]*Department of Chemistry and Centre for Self-Assembled Chemical Structures, McGill University, 801 Sherbrooke Str. West, Montreal, QC H3A 2K6, Canada. E-mail: dmitrii.perepichka@mcgill.ca*
† Electronic supplementary information (ESI) available: Synthesis of **2**, natural bond orbital analysis, additional STM images. See DOI: 10.1039/c2nr31648j

Downloaded by Institut nationale de la recherche scientifique (INRS) on 17 September 2012
Published on 16 August 2012 on http://pubs.rsc.org | doi:10.1039/C2NR31648J

of attractive interactions between the non-spherical potentials of the X-atoms. A peculiar interaction is depicted in Fig. 1c, in which an additional H-bond is formed. This X_2H three-centre motif has been observed in the literature for different molecules in 2D and 3D crystals.[28,39,40] The particular electrostatic potential also allows for interactions between three X-atoms in an X_3 synthon (Fig. 1d).[42,45,46] Note, however, that dispersion forces are likewise necessary for a complete description of X-bonds.[47]

Recently we communicated[28] that the brominated organic semiconductor tetrathienoanthracene (**1**, Fig. 2, with electrostatic potential ESP)[48–50] assembles at the liquid–solid interface into a two-dimensional network stabilized primarily by weak Br···Br and Br···H bonds.

Here we report a complete study on a series of structurally related brominated π-conjugated molecules 2,5,9,12-tetrabromoanthra[1,2-*b*:4,3-*b*′:5,6-*b*″:8,7-*b*‴]tetrathiophene **1**, 2,5,9,12-tetrabromoanthra[2,1-*b*:3,4-*b*′:6,5-*b*″:7,8-*b*‴]tetrathiophene **2** and 2,5,8-tribromobenzo[1,2-*b*:3,4-*b*′:5,6-*b*″]trithiophene **3** (Fig. 2) to show the universal nature of stabilizing bonds between halogen atoms in 2D molecular self-assembly. Using STM imaging and DFT modelling, we demonstrate how tuning the molecular structure of three organic semiconductors defines the geometry of 2D self-assembled monolayers through the interplay of X-bonds and H-bonds. A combined halogen···halogen and hydrogen···halogen three-centre binding motif (*cf.* Fig. 1c), in which the H-bond is formed close to orthogonal to the X-bond, seems to be the most important interaction scheme. We also observe the X_6 synthon (Fig. 1e) which has not been previously reported.

In addition, we investigate the semiconducting properties of **1** and **2** in organic field-effect transistors (OFET) and analyze the influence of the sulphur heteroatom position on the hole mobility.

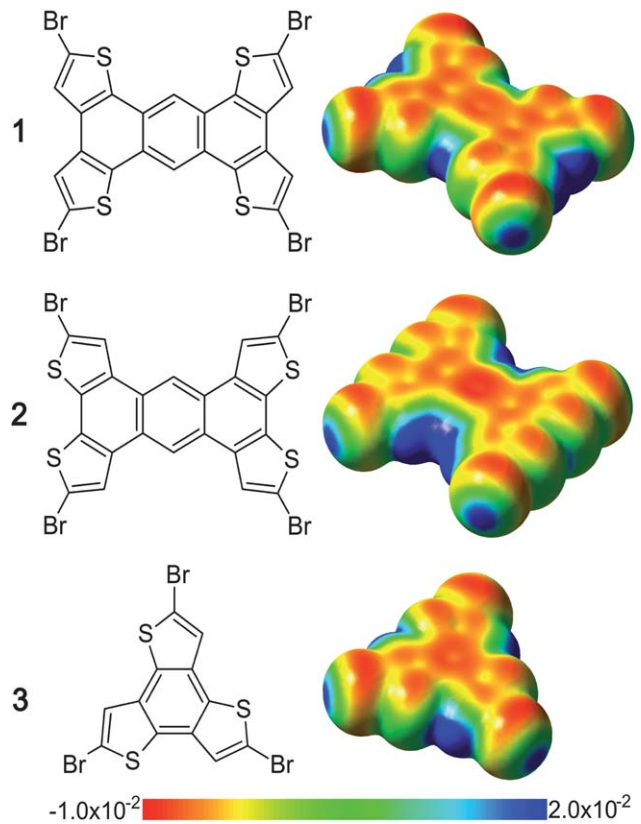

Fig. 2 Structural formula and electrostatic potential map of molecules **1**, **2**, and **3**. The ESP of all molecules shows the characteristic positive σ-hole at the peripheral parts of the bromine atoms (blue cap) and the negative equatorial belt (red ring). Lone pairs on the sulphur atoms appear perpendicular to the molecular plane in red. Hydrogen is accompanied by a positive potential.

Methods

Synthesis

Compounds **1** and **3** were synthesized as reported in ref. 49 and ref. 51, respectively. The synthesis of **2** is described in ESI.†

Scanning tunnelling microscopy

Experiments were performed using a scanning tunnelling microscope (Digital Instruments Inc. (Veeco), NanoScope IIIa) at the liquid–solid interface under ambient conditions in constant current mode. Highly oriented pyrolytic graphite (HOPG) was used as the substrate. Saturated solutions of **1** and **2** in 1,2,4-trichlorobenzene (TCB) were prepared at room temperature. The solution of **3** was heated during solvation and subsequently cooled to room temperature, which yielded an orange suspension. Drops of solution (suspension) were applied to freshly cleaved HOPG and the cut Pt–Ir STM tip immersed into the solution for scanning. Unit cells were measured in images were both the supramolecular network and the graphite surface were recorded by changing tunnelling parameters.

Computational methods

Gaussian 09 (ref. 52) was employed for density functional theory calculations applying the 6-31G(d,p) basis set. Functionals used were B3LYP, M06-L, M06-2X, B97D, and ωB97X-D. Except for B3LYP,[53] which is included for the sake of comparison, these functionals comprise dispersion interactions. M06-L and M06-2X were parameterized to account for long-range interactions,[54,55] while B97D[56] and ωB97X-D[57] include an empirical term to account for dispersion interactions. The use of different functionals is motivated by the fact that a "correct" description of dispersion interactions in the DFT framework is complicated. Consistent results from different functionals facilitate their interpretation. An approach using different functionals was previously used to assess the correct description of thermondynamics in halogen bonding by DFT.[58] Calculations were performed with periodic boundary conditions (PBC) to mimic the 2D crystalline nature of the observed structures. During optimization both lattice vectors and atom positions were free to relax in-plane. The coordinates perpendicular to the plane of the unit cell were fixed to ensure planar structures. Counterpoise-corrected binding energies are reported to accommodate the basis set superposition error (BSSE).[59,60] The use of counterpoise correction for BSSE, especially for weak interactions, is discussed controversial in literature (see ref. 61 and 62 for a concise discussion). Corrected binding energies do not necessarily give better results than uncorrected values. Nevertheless, we include both corrected and uncorrected values in our discussion for the sake of comparison with other studies. ESP maps were computed for all three molecules with the M06-2X functional.

 This journal is © The Royal Society of Chemistry 2012

Downloaded by Institut nationale de la recherche scientifique (INRS) on 17 September 2012
Published on 16 August 2012 on http://pubs.rsc.org | doi:10.1039/C2NR31648J

Device fabrication

Organic thin-film transistors (OTFTs) were prepared in top-contact configuration with symmetric Au electrodes as drain and source thermally evaporated through a shadow mask. Thin films of both **1** and **2** were grown by vacuum deposition (10^{-6} mbar, deposition rate 0.2–0.3 Å s^{-1}) on hexamethyldisilazane treated SiO_2/Si at room temperature. SiO_2 was thermally grown (200 nm thick) on heavily n-doped (Sb) Si ($\rho \approx 0.01$ Ohm cm). The performance of the resulting devices was measured in vacuum using a Keithley 4200-SCS.

Results and discussion

The semiconducting properties of **1** and **2** were tested by fabricating OFETs with vacuum-deposited thin-films of the molecules. The transistor output and transfer characteristics are shown in Fig. 3. The preliminary studies show (unoptimized) hole mobilities of 1.0×10^{-4} cm^2 V^{-1} s^{-1} and 2.3×10^{-3} cm^2 V^{-1} s^{-1} for **1** and **2**, respectively, on–off ratios of 1×10^3 and 2×10^3, and threshold voltages of −10 V and −15 V. A higher value for the mobility of **2** is in line with the OFET-mobility of hexylated version of **2** *vs.* hexylated version of **1**, where the stronger intermolecular S···S contacts in the 3D crystal structure of the **2** isomers was speculated as the reason for the better charge transport property.[49] This assumption is also consistent with the 2D structures of **1** and **2** reported here, although we do not expect an exact one-to-one correspondence between 3D structure in the bulk of the OFET and the 2D monolayer. As discussed below, the monolayer of **2** comprises multiple S···S intermolecular interactions in each unit cell, whereas the **1** cell comprises only a single S···S bond.

The three molecules each self-assemble readily into an ordered pattern when their trichlorobenzene solutions are placed on a freshly cleaved HOPG crystal. STM imaging at the solid–liquid interface reveals the different arrangements of the molecules in a monolayer and DFT calculations help in connecting these differences to the molecular structures.

Compound **1** arranges into a crystalline layer with an oblique unit cell that contains one molecule with lattice parameters $a = (1.1 \pm 0.1)$ nm, $b = (1.5 \pm 0.1)$ nm, $\gamma = (66 \pm 2)°$ (Fig. 4a). Here and in the following cases, the uniform electron density that evenly spreads over the aromatic molecule and which gives a uniform contrast in STM, together with the close packing of molecules on the surface, makes the identification of single molecules a difficult task. The adsorption geometry can be deduced from position and shape of single-molecule or dimer defect sites in the monolayer.[28] Several close contacts between bromine, sulphur, and hydrogen with a bond distance smaller than the sum of the van-der-Waals radii Σ_{vdW} are identified ($\Sigma_{vdW} = 3.70$ Å for Br···Br, 3.05 Å for Br···H, 3.65 Å for Br···S, and 3.60 Å for S···S, based on radii from ref. 63). Br···Br halogen bonds and Br···H halogen–hydrogen are the most dominant interactions stabilizing the 2D self-assembled structure. The

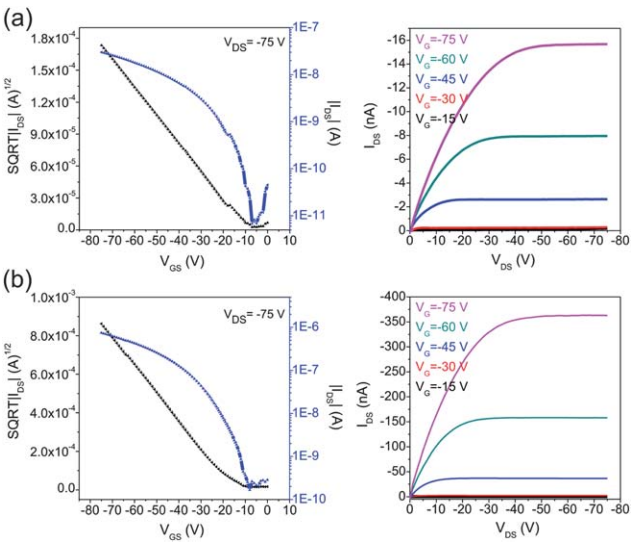

Fig. 3 Transfer (left) and output (right) characteristics of OFET built with compound **1** (a) and **2** (b) vacuum-sublimed on SiO_2/Si substrates. $W/L = 1000/100$ (μm/μm).

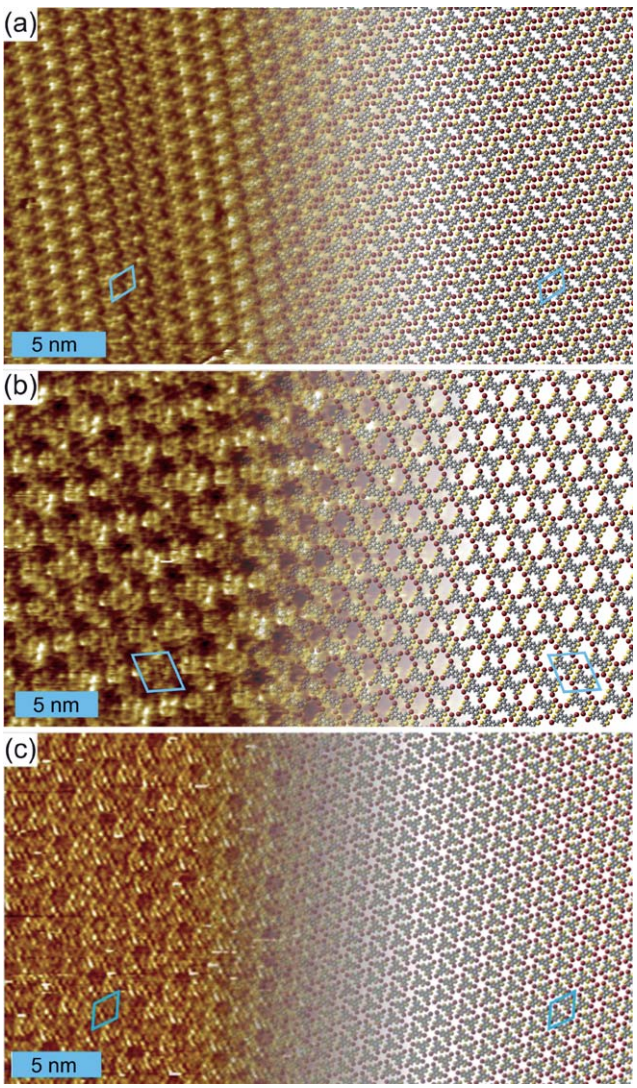

Fig. 4 STM images of the self-assembled monolayer with overlaid molecular models (a) **1** ($I_T = 100$ pA, $U_{bias} = -800$ mV), (b) **2** ($I_T = 300$ pA, $U_{bias} = -450$ mV), and (c) **3** ($I_T = 350$ pA, $U_{bias} = 800$ mV). For each structure a unit cell is indicated in blue.

Table 1 Unit cell dimensions, close-contact distances *D* between two adjacent molecules, and binding energy for **1**

	a/nm	*b*/nm	γ	*D*1[a] Br···Br/Å	*D*2 Br···H/Å	*D*3 Br···S/Å	*D*4 Br···S/Å	*D*5 Br···H/Å	*D*6 S···S/Å	Binding energy/ kcal mol^{-1}	Binding energy counterpoise corrected/ kcal mol^{-1}
M06-L	1.11	1.42	68°	3.38	2.93	3.41	3.64	2.87	3.52	−25.8	−5.1
M06-2X	1.11	1.42	68°	3.42	2.95	3.41	3.64	2.86	3.49	−25.0	−3.1
B97D	1.16	1.46	72°	3.77	3.10	3.60	4.28	3.48	4.11	−24.4	−8.9
ωB97X-D	1.13	1.43	70°	3.59	2.97	3.47	3.86	3.09	3.71	−24.9	−6.2
B3LYP	1.14	1.44	71°	3.66	2.99	3.49	4.06	3.25	3.85	−12.7	5.3

[a] Labels as shown in Fig. 5a.

Downloaded by Institut nationale de la recherche scientifique (INRS) on 17 September 2012
Published on 16 August 2012 on http://pubs.rsc.org | doi:10.1039/C2NR31648J

computational results are summarized in Table 1, and the calculated structure is shown in Fig. 5a. For simplicity only numbers calculated with the M06-2X functional will be discussed here. A comparison with the other functionals will be given at the end of this section. The lateral dimensions of the experimental unit cell are reproduced in the calculations. The most significant close-contacts are *D*1 Br···Br, *D*2 Br···H, and *D*4 Br···S (see Fig. 5a), where almost all functionals yield values smaller than Σ_{vdW}. *D*1 measures 3.42 Å (calculated with M06-2X functional) compared to 3.676 Å measured by X-ray analysis of a single crystal of **1**.[64] The difference between the 3D experimental values and theoretical numbers might be due to different molecular packing, a possible underestimation of bond length in the chosen functional, or both. The uncorrected binding energy amounts to about −25.0 kcal mol^{-1}.

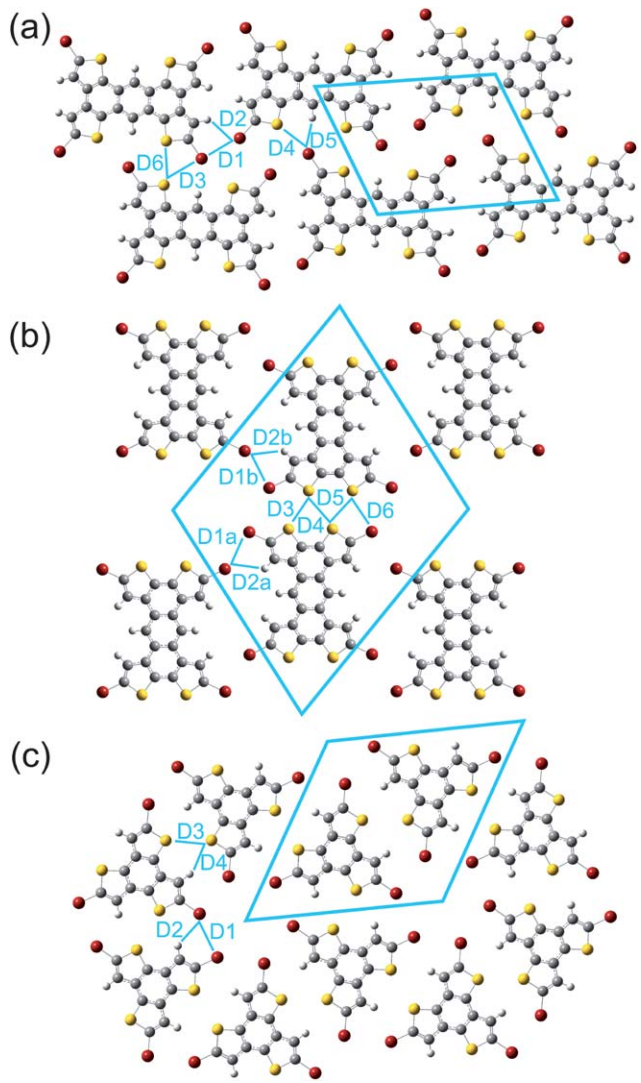

Fig. 5 Model of the three different monolayers showing the unit cell in blue and the close contacts that stabilize the structure. (a) **1**, (b) **2**, and (c) **3**. The labels *D*1 to *D*6 correspond to the nomenclature in the Tables 1–3 for each molecule. Grey: carbon, white: hydrogen, yellow: sulphur, red: bromine.

The intermolecular interactions are understandable from the ESP of **1**. The parts of the molecule with positive potential point towards parts of neighbouring molecules with negative potential, thus executing a positive electrostatic attraction. This scheme can be found, for example, in the attraction of the negative equatorial part of bromine by the positive cap of another bromine in the typical Br···Br bond.

The same interactions are found in the self-assembly of **2**. It assembles in a structure with an oblique unit cell that measures $a = (1.9 \pm 0.1)$ nm, $b = (1.9 \pm 0.1)$ nm, $\gamma = (108 \pm 2)°$ and which contains two molecules (Fig. 4b). DFT calculations yield an asymmetric unit cell with $a \approx 1.9$ nm, $b \approx 2.1$ nm, $\gamma = 108°$, as reported in Table 2. The apparent discrepancy with experiment might be due to the influence of the substrate, which was not taken into account in our calculations. Six close contacts smaller than Σ_{vdW} can be identified (see Fig. 5b). Out of these, the Br···Br contacts *D*1a and *D*1b are smaller than Σ_{vdW}, as well as the S···S contacts *D*3, *D*4, and *D*5, and the S···Br contact *D*6. The same S···S interactions spanned by the *D*3, *D*4, and *D*5 are found in 3D crystals of the non-brominated version of **2**.[49] The measured distances amount to $D3_{3D} = 3.635$ Å, $D4_{3D} = 3.773$ Å, and $D5_{3D} = 3.719$ Å. These are somewhat larger than the calculated values of $D3 = D5 = 3.42$ Å and $D4 = 3.57$. Again, the discrepancy can be attributed to a difference between strictly planar 2D and non-planar 3D assembly, and the additional X-bonds which are present in 2D for **2** but absent in the 3D crystal for the non-brominated counterpart. The Br···H contacts *D*2a and *D*2b are larger than the sum of the van-der-Waals radii. Despite this large separation, natural bond orbital (NBO, see ESI†) analysis shows small attractive charge transfer interactions for *D*2a and *D*2b. The three-centre bond spanned by *D*1 and *D*2 is the basis of the X_2H synthon shown in Fig. 1c. The geometry is similar to the same bonding configuration between two bromine atoms and hydrogen found for **1** and is the driving force in the self-assembly process. Although the **2** monolayer is stabilized by the same interactions as

 This journal is © The Royal Society of Chemistry 2012

Table 2 Unit cell dimensions, close-contact distances *D* between two adjacent molecules, and binding energy for **2**

	a/nm	*b*/nm	γ	*D*1a[a] Br···Br/Å	*D*2a Br···H/Å	*D*1b Br···Br/Å	*D*2b Br···H/Å	*D*3 S···S/Å	*D*4 S···S/Å	*D*5 S···S/Å	*D*6 S···Br/Å	Binding energy/ kcal mol^{-1}	Binding energy counterpoise corrected/ kcal mol^{-1}
M06-L	1.88	2.08	107°	3.47	3.24	3.41	3.63	3.44	3.58	3.44	3.60	−12.8	−2.0
M06-2X	1.89	2.08	109°	3.49	3.14	3.50	3.14	3.42	3.57	3.42	3.58	−13.5	−1.3
B97D	1.95	2.16	108°	3.59	3.61	3.59	3.65	3.96	3.95	3.96	4.03	−13.3	−4.4
ωB97X-D	1.91	2.10	108°	3.52	3.40	3.52	3.44	3.59	3.72	3.59	3.75	−13.5	−2.9
B3LYP	1.92	2.12	107°	3.53	3.54	3.53	3.65	3.73	3.81	3.73	3.87	−6.9	3.1

[a] Labels as shown in Fig. 5b.

Downloaded by Institut nationale de la recherche scientifique (INRS) on 17 September 2012
Published on 16 August 2012 on http://pubs.rsc.org | doi:10.1039/C2NR31648J

the **1** monolayer, its binding energy is lower, possibly due to electrostatic repulsion in the additional close S···S contacts. The uncorrected binding energy is about −13.5 kcal mol^{-1}. These results are summarized in Table 2.

The third molecule, compound **3**, assembles into a hexagonal structure (Fig. 4c). The unit cell measures $a = (1.4 \pm 0.1)$ nm, $b = (1.4 \pm 0.1)$ nm, $\gamma = (60 \pm 2)°$. The molecules arrange into six-membered rings that densely cover the surface. The centre of each of these rings contains six Br atoms belonging to the six different molecules. Halogen–halogen bonds stabilize the rings. Further lateral stabilization between adjacent molecules is due to Br···H and S···S contacts, as shown in Fig. 5c. DFT calculations (Table 3) give an optimized unit cell close to the observed one within experimental error. Close contacts smaller than Σ_{vdW} are Br···Br, Br···H, and S···S. Here again, the X_2H synthon can be found between *D*1 and *D*2. The uncorrected binding energy is −13.9 kcal mol^{-1}. Compound **3** assembles into small domains compared with **1**. The structures are not very stable and dissolve and reappear during imaging. It is interesting to note the circular interaction of six bromine atoms (along the *D*1 contact, see Fig. 5c), which is due to the simultaneous nuclephilic and electrophilic character of the X-atom. Circular X_3 halogen bonding (*cf.* Fig. 1d) has been reported previously,[45,30] but none is known to us which comprises six halogen atoms in a X_6 synthon, as observed in the **3** monolayer (although it might be the underlying binding motif of tris(*p*-bromophenyl)-benzene at low temperature[30]). The X_6 binding motif is topologically similar to the $R_6^6(24)$ binding motif encountered at the liquid–solid interface for the carboxylated version of **3**.[18]

All three ordered self-assembled monolayers are stabilized by weak interaction between bromine, hydrogen, and sulphur. The close contacts that are the dominant ones according to DFT calculations are shown in a model in Fig. 5. The Br···Br and Br···H bonds are found to be especially important, but S···S and Br···S interactions also contribute. The former two bonds are explainable on the basis of the electrostatic potential of the three molecules. The positive cap of the Br atom points towards the negative ring in an adjacent Br atom and exercises an attractive force in a Br···Br bond, just as partially positive hydrogen can be attracted by the negative ring similar to a hydrogen bond. The Br atom interacts at the same time with hydrogen (electrophile) and with the negative ring of an adjacent Br atom (nucleophile). The electrostatic potential maps for the molecules that are depicted in Fig. 2 together with the geometrical arrangement of the molecules in the monolayers show how parts with positive and negative potential in the molecules attract each other. The Br···S bonds in the **1** and **2** structures are stabilized by charge donation from the S lone-pairs into the C–Br σ^* antibonding orbital.[28] The S···S chalcogen bonds are weakly stabilized by charge donation from lone-pairs to C–S σ^* antibonding orbitals (see ESI† for NBO analysis and ref. 65). Neglecting interaction with the substrate, **3** and **2** were found to have similar binding energies within their respective monolayers, whereas **1** has a binding energy almost twice as large. Monolayers of **3** show a fluctuating nature of its domains with a smaller domain size than **1** and **2** (see ESI†). Differences in binding energy within the monolayer can be excluded as responsible for this observation since **2** and **3** show the same binding energy but different domain sizes. Reasons for the small domains can be smaller interactions of **3** with the graphite lattice due to its smaller size compared to **1** and **2**, or a different adsorption–desorption equilibrium. This last point is underlined by the necessity to use supersaturated solutions of **3** to observe molecules on the surface, while saturated solutions of **1** and **2** suffice.

All five functionals used in the DFT calculations give consistent results for the geometry of the monolayer (compare Tables 1–3). The unit cells differ by less than 0.2 nm in lateral dimension and by less than 4° in angle (less than 2° excluding **1** calculated with B97D, the only case in which the difference is 4°). The close contacts between Br, S, and H, however, show a larger deviation,

Table 3 Unit cell dimensions, close-contact distances *D* between two adjacent molecules, and binding energy for **3**

	a/nm	*b*/nm	γ	*D*1[a] Br···Br/Å	*D*2 Br···H/Å	*D*3 S···S/Å	*D*4 S···H/Å	Binding energy/ kcal mol^{-1}	Binding energy counterpoise corrected/kcal mol^{-1}
M06-L	1.52	1.52	60°	3.64	2.99	3.52	3.01	−13.8	−3.3
M06-2X	1.52	1.52	60°	3.63	2.98	3.51	3.09	−13.9	−2.5
B97D	1.60	1.60	60°	4.07	3.26	3.77	3.55	−14.1	−6.2
ωB97X-D	1.54	1.54	60°	3.78	3.08	3.60	3.25	−14.7	−4.6
B3LYP	1.56	1.56	60°	3.88	3.15	3.65	3.37	−6.5	3.2

[a] Labels as shown in Fig. 5c.

Downloaded by Institut nationale de la recherche scientifique (INRS) on 17 September 2012
Published on 16 August 2012 on http://pubs.rsc.org | doi:10.1039/C2NR31648J

and more importantly, do not always give consistent results on whether a contact is smaller or larger than the sum of the van-der-Waals radii. The B3LYP functional, although it does not describe dispersion interactions, performs reasonably well compared to the other four functionals in predicting unit cell parameters. The major difference lies in the stabilization energies of the calculated structures. The four functionals that describe dispersion interactions give quite similar results for uncorrected values, while B3LYP underestimates energies by a factor of one half. BSSE values corrected with counterpoise correction are much smaller than uncorrected values (three to ten times smaller) and show a larger deviation between different functionals (*cf.* Tables 1–3). B3LYP even yields repulsive values for corrected energies. This leads us to the conclusion that counterpoise correction of the basis set superposition error is not an adequate method to calculate interaction energies in the halogen-bonded 2D layers.

Conclusions

We demonstrate that 2D supramolecular structures can be stabilized at the liquid–solid interface by weak interactions between halogen atoms and hydrogen atoms. Halogenated organic semiconductors with thiophene groups self-assemble into 2D monolayers and interact with each other *via* weak bonds between bromine, hydrogen, and the sulphur atoms. The electrostatic potential is a good roadmap for intermolecular interactions. We find for all three molecules that negative parts of one molecule interact with positive parts of its nearest neighbour. The intricacies and variations in the potentials of brominated thiophene-based organic semiconductors lead to a rather dense packing on the graphite surface. A newly described binding modality, the X_6 synthon, is formed by a circular arrangement of six Br atoms. For all experimentally observed structures, halogen bonding is correctly described by all functionals used in our DFT calculations that incorporate dispersion interactions. Chalcogen bonds between sulphur atoms, on the other hand, are manifested as short contacts in calculations using the M06 functionals, while the B97 functionals and B3LYP do not confirm the relevance of such an interaction. In any case, the number of these S···S interactions per unit cell correlates with the hole mobilities measured for **1** and **2** in thin film transistors. The exact molecular packing in the OFETs, however, is expected to be different from the arrangement of the molecules in the monolayer investigated here by STM.

Halogen bonding in 2D self-assembly can be used for the nanopatterning of surfaces, for example with porous networks as shown here with molecules **2** and **3**. We anticipate that networks with larger pores can be synthesized at the liquid–solid interface using different molecules, and that these networks can function as a template for the coadsorption of guest molecules.

Acknowledgements

This work is supported by the Natural Sciences and Engineering Research Council of Canada (NSERC) through Discovery Grants, as well as the Fonds Quebecois sur la Recherche en Nature et Technologies (FQRNT) through a Team Grant and the Ministère du DéveloppementEconomique, de l'Innovation et de l'Exportation (MDEIE) through an international collaboration Grant. We thank the Centre for Research in Molecular Modelling (CERMM) for access to computational infrastructure. F.R. is grateful to the Canada Research Chairs program for partial salary support.

Notes and references

1 M. Fourmigué and P. Batail, *Chem. Rev.*, 2004, **104**, 5379–5418.
2 G. R. Desiraju, *Angew. Chem., Int. Ed.*, 2007, **46**, 8342–8356.
3 F. Rosei, M. Schunack, Y. Naitoh, P. Jiang, A. Gourdon, E. Laegsgaard, I. Stensgaard, C. Joachim and F. Besenbacher, *Prog. Surf. Sci.*, 2003, **71**, 95–146.
4 O. Ivasenko and D. F. Perepichka, *Chem. Soc. Rev.*, 2011, **40**, 191–206.
5 F. Cicoira, C. Santato and F. Rosei, *Top. Curr. Chem.*, 2008, **285**, 203–267.
6 J. A. A. W. Elemans and S. de Feyter, *Soft Matter*, 2009, **5**, 721–735.
7 J. A. A. W. Elemans, S. Lei and S. D. Feyter, *Angew. Chem., Int. Ed.*, 2009, **48**, 7298–7332.
8 L. Bartels, *Nat. Chem.*, 2010, **2**, 87–95.
9 A. Ciesielski, C.-A. Palma, M. Bonini and P. Samorì, *Adv. Mater.*, 2010, **22**, 3506–3520.
10 K. Tahara, S. Furukawa, H. Uji-i, T. Uchino, T. Ichikawa, J. Zhang, W. Mamdouh, M. Sonoda, F. C. De Schryver, S. De Feyter and Y. Tobe, *J. Am. Chem. Soc.*, 2006, **128**, 16613–16625.
11 Q. Chen, H. Yan, C. Yan, G. Pan, L. Wan, G. Wen and D. Zhang, *Surf. Sci.*, 2008, **602**, 1256–1266.
12 K. S. Mali, K. Lava, K. Binnemans and S. De Feyter, *Chem.–Eur. J.*, 2010, **16**, 14447–14458.
13 P. N. Dickerson, A. M. Hibberd, N. Oncel and S. L. Bernasek, *Langmuir*, 2010, **26**, 18155–18161.
14 K. G. Nath, O. Ivasenko, J. A. Miwa, H. Dang, J. D. Wuest, A. Nanci, D. F. Perepichka and F. Rosei, *J. Am. Chem. Soc.*, 2006, **128**, 4212–4213.
15 K. G. Nath, O. Ivasenko, J. M. MacLeod, J. A. Miwa, J. D. Wuest, A. Nanci, D. F. Perepichka and F. Rosei, *J. Phys. Chem. C*, 2007, **111**, 16996–17007.
16 J. M. MacLeod, O. Ivasenko, D. F. Perepichka and F. Rosei, *Nanotechnology*, 2007, **18**, 424031.
17 M. Lackinger and W. M. Heckl, *Langmuir*, 2009, **25**, 11307–11321.
18 J. M. MacLeod, O. Ivasenko, C. Fu, T. Taerum, F. Rosei and D. F. Perepichka, *J. Am. Chem. Soc.*, 2009, **131**, 16844–16850.
19 H. Wang, T. E. Kaiser, S. Uemura and F. Würthner, *Chem. Commun.*, 2008, 1181–1183.
20 R. Gutzler, S. Lappe, K. Mahata, M. Schmittel, W. M. Heckl and M. Lackinger, *Chem. Commun.*, 2009, 680–682.
21 S.-L. Lee, N.-T. Lin, W.-C. Liao, C.-H. Chen, H.-C. Yang and T.-Y. Luh, *Chem.–Eur. J.*, 2009, **15**, 11594–11600.
22 P. Metrangolo, H. Neukirch, T. Pilati and G. Resnati, *Acc. Chem. Res.*, 2005, **38**, 386–395.
23 F. F. Awwadi, R. D. Willett, K. A. Peterson and B. Twamley, *Chem.–Eur. J.*, 2006, **12**, 8952–8960.
24 A. C. Legon, *Phys. Chem. Chem. Phys.*, 2010, **12**, 7736–7747.
25 X. Yang, F. Wang, Q. Chen, L. Wang and Z. Wang, *Chin. Sci. Bull.*, 2007, **52**, 1856–1859.
26 Q. Chen, T. Chen, X. Zhang, L.-J. Wan, H.-B. Liu, Y.-L. Li and P. Stang, *Chem. Commun.*, 2009, 3765–3767.
27 Q. Chen, T. Chen, D. Wang, H.-B. Liu, Y.-L. Li and L.-J. Wan, *Proc. Natl. Acad. Sci. U. S. A.*, 2010, **107**, 2769–2774.
28 R. Gutzler, O. Ivasenko, C. Fu, J. L. Brusso, F. Rosei and D. F. Perepichka, *Chem. Commun.*, 2011, **47**, 9453–9455.
29 J. C. Russell, M. O. Blunt, J. M. Garfitt, D. J. Scurr, M. Alexander, N. R. Champness and P. H. Beton, *J. Am. Chem. Soc.*, 2011, **133**, 4220–4223.
30 H. Walch, R. Gutzler, T. Sirtl, G. Eder and M. Lackinger, *J. Phys. Chem. C*, 2010, **114**, 12604–12609.
31 J. K. Yoon, W.-J. Son, K.-H. Chung, H. Kim, S. Han and S.-J. Kahng, *J. Phys. Chem. C*, 2011, **115**, 2297–2301.
32 K.-H. Chung, J. Park, K. Y. Kim, J. K. Yoon, H. Kim, S. Han and S.-J. Kahng, *Chem. Commun.*, 2011, **47**, 11492–11494.
33 S. M. Clarke, T. Friščić, W. Jones, A. Mandal, C. Sun and J. E. Parker, *Chem. Commun.*, 2011, **47**, 2526–2528.

 This journal is © The Royal Society of Chemistry 2012

View Online

34 S. Schlögel, T. Sirtl, J. Eichhorn, W. M. Heckl and M. Lackinger, *Chem. Commun.*, 2011, **47**, 12355–12357.
35 T. Shirman, D. Freeman, Y. D. Posner, I. Feldman, A. Facchetti and M. E. van der Boom, *J. Am. Chem. Soc.*, 2008, **130**, 8162–8163.
36 T. Shirman, R. Kaminker, D. Freeman and M. E. van der Boom, *ACS Nano*, 2011, **5**, 6553–6563.
37 M. L. Tang and Z. Bao, *Chem. Mater.*, 2011, **23**, 446–455.
38 A. R. Voth, P. Khuu, K. Oishi and P. S. Ho, *Nat. Chem.*, 2009, **1**, 74–79.
39 O. Navon, J. Bernstein and V. Khodorkovsky, *Angew. Chem., Int. Ed. Engl.*, 1997, **36**, 601–603.
40 H. F. Lieberman, R. J. Davey and D. M. T. Newsham, *Chem. Mater.*, 2000, **12**, 490–494.
41 M. Bonini, L. Zalewski, E. Orgiu, T. Breiner, F. Dötz, M. Kastler and P. Samorì, *J. Phys. Chem. C*, 2011, **115**, 9753–9759.
42 C. M. Reddy, M. T. Kirchner, R. C. Gundakaram, K. A. Padmanabhan and G. R. Desiraju, *Chem.–Eur. J.*, 2006, **12**, 2222–2234.
43 T. T. T. Bui, S. Dahaoui, C. Lecomte, G. R. Desiraju and E. Espinosa, *Angew. Chem., Int. Ed.*, 2009, **48**, 3838–3841.
44 T. Clark, M. Hennemann, J. Murray and P. Politzer, *J. Mol. Model.*, 2007, **13**, 291–296.
45 E. Bosch and C. L. Barnes, *Cryst. Growth Des.*, 2002, **2**, 299–302.
46 Y. Lu, J. Zou, H. Wang, Q. Yu, H. Zhang and Y. Jiang, *J. Phys. Chem. A*, 2005, **109**, 11956–11961.
47 K. E. Riley and P. Hobza, *J. Chem. Theory Comput.*, 2008, **4**, 232–242.
48 W.-J. Liu, Y. Zhou, Y. Ma, Y. Cao, J. Wang and J. Pei, *Org. Lett.*, 2007, **9**, 4187–4190.
49 J. L. Brusso, O. D. Hirst, A. Dadvand, S. Ganesan, F. Cicoira, C. M. Robertson, R. T. Oakley, F. Rosei and D. F. Perepichka, *Chem. Mater.*, 2008, **20**, 2484–2494.
50 F. He, W. Wang, W. Chen, T. Xu, S. B. Darling, J. Strzalka, Y. Liu and L. Yu, *J. Am. Chem. Soc.*, 2011, **133**, 3284–3287.
51 T. Taerum, O. Lukoyanova, R. G. Wylie and D. F. Perepichka, *Org. Lett.*, 2009, **11**, 3230–3233.
52 M. J. Frisch, G. W. Trucks, H. B. Schlegel, G. E. Scuseria, M. A. Robb, J. R. Cheeseman, G. Scalmani, V. Barone, B. Mennucci, G. A. Petersson, H. Nakatsuji, M. Caricato, X. Li, H. P. Hratchian, A. F. Izmaylov, J. Bloino, G. Zheng, J. L. Sonnenberg, M. Hada, M. Ehara, K. Toyota, R. Fukuda, J. Hasegawa, M. Ishida, T. Nakajima, Y. Honda, O. Kitao, H. Nakai, T. Vreven, J. A. Montgomery Jr, J. E. Peralta, F. Ogliaro, M. Bearpark, J. J. Heyd, E. Brothers, K. N. Kudin, V. N. Staroverov, R. Kobayashi, J. Normand, K. Raghavachari, A. Rendell, J. C. Burant, S. S. Iyengar, J. Tomasi, M. Cossi, N. Rega, J. M. Millam, M. Klene, J. E. Knox, J. B. Cross, V. Bakken, C. Adamo, J. Jaramillo, R. Gomperts, R. E. Stratmann, O. Yazyev, A. J. Austin, R. Cammi, C. Pomelli, J. W. Ochterski, R. L. Martin, K. Morokuma, V. G. Zakrzewski, G. A. Voth, P. Salvador, J. J. Dannenberg, S. Dapprich, A. D. Daniels, Ö. Farkas, J. B. Foresman, J. V. Ortiz, J. Cioslowski and D. J. Fox, *Gaussian 09*, Gaussian, Inc., Wallingford CT, 2009.
53 A. D. Becke, *J. Chem. Phys.*, 1993, **98**, 5648–5652.
54 Y. Zhao and D. Truhlar, *Theor. Chim. Acta*, 2008, **120**, 215–241.
55 Y. Zhao and D. G. Truhlar, *Acc. Chem. Res.*, 2008, **41**, 157–167.
56 S. Grimme, *J. Comput. Chem.*, 2006, **27**, 1787–1799.
57 J.-D. Chai and M. Head-Gordon, *Phys. Chem. Chem. Phys.*, 2008, **10**, 6615–6620.
58 M. G. Chudzinski and M. S. Taylor, *J. Org. Chem.*, 2012, **77**, 3483–3491.
59 S. F. Boys and F. Bernardi, *Mol. Phys.*, 1970, **19**, 553–566.
60 J. P. Bowen, J. B. Sorensen and K. N. Kirschner, *J. Chem. Educ.*, 2007, **84**, 1225–1229.
61 J. R. Alvarez-Idaboy and A. Galano, *Theor. Chem. Acc.*, 2009, **126**, 75–85.
62 X. W. Sheng, L. Mentel, O. V. Gritsenko and E. J. Baerends, *J. Comput. Chem.*, 2011, **32**, 2896–2901.
63 A. Bondi, *J. Phys. Chem.*, 1964, **68**, 441–451.
64 A. A. Leitch, A. Mansour, K. A. Stobo, I. Korobkov and J. L. Brusso, *Cryst. Growth Des.*, 2012, **12**, 1416–1421.
65 R. Gleiter, D. B. Werz and B. J. Rausch, *Chem.–Eur. J.*, 2003, **9**, 2676–2683.

Downloaded by Institut nationale de la recherche scientifique (INRS) on 17 September 2012
Published on 16 August 2012 on http://pubs.rsc.org | doi:10.1039/C2NR31648J